Journal of Applied Physics

Nanopowder management and control of plasma parameters in electronegative SiH_4 plasmas

Cite as: Journal of Applied Physics **94**, 6097 (2003); https://doi.org/10.1063/1.1618356
Submitted: 14 May 2003 . Accepted: 19 August 2003 . Published Online: 23 October 2003

I. B. Denysenko, K. Ostrikov, S. Xu, M. Y. Yu, and C. H. Diong

Nanopowder management and control of plasma parameters in electronegative SiH_4 plasmas

I. B. Denysenko[a)]
Plasma Sources and Applications Center, NIE, Nanyang Technological University, 637 616 Singapore

K. Ostrikov
School of Physics, The University of Sydney, NSW 2006, Sydney, Australia and Plasma Sources and Applications Center, NIE, Nanyang Technological University, 637 616 Singapore and SOCPES, Flinders University, GPO Box 2100, Adelaide SA 5001, Australia

S. Xu[b)]
Plasma Sources and Applications Center, NIE, Nanyang Technological University, 637 616 Singapore

M. Y. Yu
Theoretical Physics I, Ruhr University, D-44780 Bochum, Germany

C. H. Diong
Natural Sciences, NIE, Nanyang Technological University, 637 616 Singapore

(Received 14 May 2003; accepted 19 August 2003)

Management of nanosize powder particles via control of plasma parameters in a low-pressure SiH_4 discharge for silicon microfabrication technologies is considered. The spatial profiles of electron and positive/negative ion number densities, electron temperature, and charge of the fine particles are obtained using a self-consistent fluid model of the electronegative plasmas in the parallel plate reactor geometry. The model accounts for variable powder size and number density, powder-charge distribution, local plasma nonuniformity, as well as UV photodetachment of electrons from the nanoparticles. The relations between the equilibrium discharge state and powder properties and the input power and neutral gas pressure are studied. Methods for controlling the electron temperature and SiH_3^- anion (here assumed to be the powder precursor) density, and hence the powder growth process, are proposed. It is shown that by controlling the neutral gas pressure, input power, and powder size and density, plasma density profiles with high levels of uniformity can be achieved. Management of powder charge distribution is also possible through control of the external parameters. © *2003 American Institute of Physics.* [DOI: 10.1063/1.1618356]

I. INTRODUCTION

Generation of particulates ranging in size from nanometers up to tens of microns has been observed in many processing plasmas used in the semiconductor industry.[1–4] The fine particles, or powder, can be detrimental in dry etching and deposition for manufacturing ultra-large scale integrated (ULSI) functionalities and devices. These so-called killer particles, tend to deposit on the wafer during the processing and can adversely affect the designed features of the integrated circuitry.

On the other hand, for manufacturing certain electronic materials[5] the presence of fine particulates in the plasma is desired or beneficial.[6] For example, powder agglomeration (the γ regime) is often utilized in plasma enhanced chemical vapor deposition (PECVD),[7] since the powder enhanced plasma chemistry and lowered sheath potentials can lead to faster deposition rates and lower defect densities.[8] Processing of plasma produced and trapped or externally injected fine particles in plasmas can be useful in fabricating objects such as coated or layered grains with specific surface structure, color, and/or fluorescent properties,[1,9] or nanostructured surfaces with the required properties.[6,10–12] The integrated process of nanoparticle creation and ordered deposition of the processed objects is one of the most promising methods for the synthesis of new composite materials.[6] Plasma grown nanopowder can be used to modify the structure–property relationships, domain structure, and growth dynamics in the integration of various epitaxial oxide and other films on silicon-based nanostructures.[13–15] The powder particles can also affect the nucleation of ultrafine crystallites in amorphous silicon-based films,[16] as well as the thermoelectric and other properties of silicon-based films in silicon on insulator (SOI) and other microfabrication technologies.[17]

In practical applications, it is often necessary to control, or manage, the size, density, electrical charge, and transport characteristics of the powder.[6] For example, powder size management is crucial in low-temperature deposition of polymorphous and polycrystalline silicon films.[10,18–20] In particular, growth of silicon clusters and crystallites, while avoiding their agglomeration, is often desired.[10] In ULSI manufacturing, to minimize the harmful effects of the nano-

a)Permanent address: School of Physics and Technology, Kharkiv National University, 4 Svobody sq., 61077 Kharkiv, Ukraine.
b)Author to whom correspondence should be addressed; electronic mail: syxu@nie.edu.sg

particles it is necessary to either suppress powder generation[21] or transport/filter the contaminant particles out of the processing volume.[22–24] One can then develop process cycles such that the substrate regions sensitive to powder fallout are free of contaminated plasma.[4] To this effect powder charge management is important since the charge of the particles determines both their confinement and their motion to or from the processed surface.

Nanometer sized powder particles or grains are usually generated inside the plasma from precursors, and the plasma determines the powder properties. Therefore, powder management is possible only through control of the plasma parameters and the chemical reactions inside the reactor. The reaction rates depend on many factors, especially the precursor density and neutral gas and electron temperatures.[25,26] Furthermore, nonlinear, nonlocal, and other complex plasma effects[27,28] can strongly affect powder formation. Thus, efficient powder management implies appropriate control of the plasma parameters.

The goal of efficient nanopowder management of chemically active processing plasmas has stimulated extensive studies of the origin and growth,[1,2,29,30] charging, and transport of fine particles (see, e.g., Refs. 31–35 and the references therein). However, most of the existing modeling efforts on the powder-containing plasmas are limited to rather simple cases of the absence of negative ions or spatial uniformity of the plasma parameters.

In this article we consider low-pressure powder-generating silane (SiH_4) plasmas often used in semiconductor manufacturing, and propose a practical model of a parallel-plate electronegative discharge containing nanopowder. In the model, it is assumed that SiH_3^- is the most abundant negative ion in the plasma and a major powder growth precursor. This assumption is supported by the data of Boufendi and Bouchoule[8] suggesting that the SiH_3^- anion-triggered clustering (via successive dissociative attachment reactions) process

$$(Si_nH_{2n+1})^- + SiH_4 \rightarrow (Si_{n+1}H_{2n+3})^- + H_2$$

can be responsible for the initial nanoparticle growth. Other mechanisms for clustering in silane plasmas involving growth kinetics through neutral and charged clusters have also been proposed.[21,29,36]

We demonstrate that nanopowder can be effectively managed through control and optimization of the plasma parameters that affect powder formation in SiH_4 electronegative discharges. In the proposed self-consistent fluid model of the electronegative parallel-plate high-density ($\geqslant 10^{10}$ cm^{-3}) plasma discharge, only relatively large nanoparticles (with size of about 10 nm) are considered. Thus, quantum effects in powder formation and charging can be ignored. To calculate the grain charge we use the conventional orbit motion limited (OML) electrostatic probe theory.[37–39]

It should be pointed out that the frequently used assumption of monodisperse dust charge fails for the size range of interest here because of large charge fluctuations.[40,41] In this case the full width at half maximum (FWHM) of the grain charge distribution function (CDF) can be comparable to the average powder charge.[37–39] We also note that earlier works on modeling of powder-containing discharges usually sidestep the intrinsic plasma nonuniformity. Furthermore, since the powder size is relatively small, UV photodetachment (UVPD) can strongly affect the grain charge distribution as well as the plasma properties.[37,42–44] In particular, the emitted photoelectron current can be so large that small grains can become positively charged.[42–45] Thus, we will obtain the CDFs taking into account the spatial variation of the plasma parameters such as the electron temperature, electron, and positive/negative ion densities. The effects of UVPD will also be considered.

We investigate the effects of power absorbed by the plasma, the neutral gas pressure, as well as photodetachment of electrons from the grains on the plasma parameters. Conditions that enable efficient electron temperature and negative ion (SiH_3^-, taken to be the powder precursor) density control, and hence particle growth, are established. The effect of the external parameters on the CDF of the nanoparticles is also studied. We show that by controlling the powder properties one can also manage the electron temperature, electron and positive/negative ion densities, and other discharge parameters. Effective methods for controlling the uniformity of the positive ion density through management of the powder properties are proposed.

This article is organized as follows. The basic assumptions, equations, and boundary conditions of the hydrodynamic model are described in Sec. II. The conditions for determining the powder CDF, as well as description of the numerical method used in the self-consistent calculation of the powder and discharge parameters are presented. Section III details the effects of the powder density and size, the external control parameters (the input power and neutral gas pressure), as well as UV photodetachment on the main discharge parameters. In Sec. IV we summarize the main results and discuss their potential importance, ways for improvement of our model are also discussed. A summary of this work and an outlook for future research are also presented.

II. DISCHARGE MODEL

Our study of electronegative plasmas loaded with nanoparticles consists of two parts which are coupled in a self-consistent numerical scheme. The parts deal with the charging of particles and the self-consistent determination of the local plasma properties, respectively. The latter include the electron and positive/negative ion densities, and the electron temperature.

A. Basic assumptions

For simplicity, we restrict our attention to a one-dimensional (1D) parallel-plate discharge geometry. It is assumed that the discharge is bounded at $x = \pm L/2$ by metal or dielectric surfaces and symmetrical with respect to midplane $x = 0$. Quasistationary plasma states are considered. The electric field sustaining the plasma is uniform along x direction.

Considering a silane SiH_4 discharge we assume that the electrons, SiH_3^+ positive ions, SiH_3^- negative ions, and the nanoparticles are the main species in the plasma. This dis-

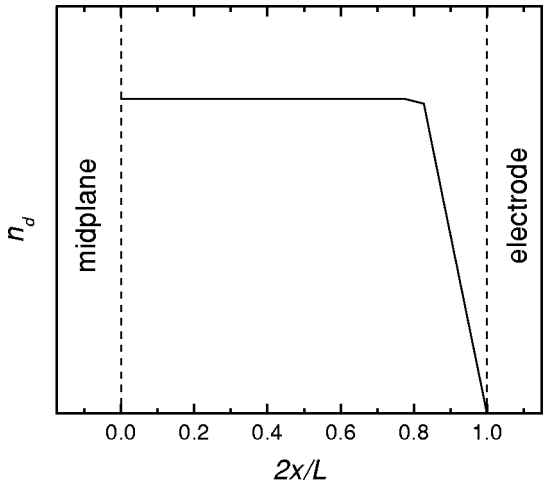

FIG. 1. Schematic diagram of the spatial profile of the powder density n_d used in computations. Here, $x=0$ corresponds to the discharge midplane.

charge modeling is based on data from typical silane-based discharges with the highest number densities of singly charged $SiH_3^{\pm}$ ions.[46] The simpler (compared to that in some other works[47,48]) species composition allows us to obtain self-consistent nonuniform profiles of the discharge parameters and CDFs of the nanopowder in a relatively simple manner. The effect of UVPD of electrons from the nanopowder on the plasma state and charge of the powder is accounted for (see, Sec. III E). We shall consider relatively large (say, 10 nm) powder, so that a quantum treatment in the calculation of the grain charge is not necessary. We shall use the conventional orbit motion limited (OML) probe theory to obtain the particle charge.[37–39]

We assume that the nanoparticles are uniformly distributed along the x axis in the center part of the discharge, and the density drops linearly to zero at the plasma boundary (Fig. 1). The profile of the powder density is chosen to fit that typically observed in the powder growth experiments.[49] The dispersion of the powder size is neglected. Since the latter have a much larger mass (a 2 nm grain contains about 1000 atoms[37]) than the other charged and neutral particles, they are treated as immobile point masses. For all the charged particles the energy distribution functions are assumed to be Maxwellian. Furthermore, the ions and neutrals are at the room temperature (300 K).

B. Electron and ion balance equations

We will use the ambipolar fluid model for the plasma, which is assumed to be in a quasineutral state. Thus, there is balance of the fluxes of the positive and negative charged particles at the grain surface

$$n_i - n_e - n_- + \Sigma_k n_d^k Z_d^k = 0, \tag{1}$$

$$\Gamma_i = \Gamma_e + \Gamma_-, \tag{2}$$

where n_α and Γ_α are density and flux of the species $\alpha = e, i$, and $-$, corresponding to electrons, positive and negative ions, respectively, n_d^k is density of the nanoparticles having the charge $Z_d^k = ke$ (with e the elementary charge and k an integer). The total dust density n_d ($=\Sigma_k n_d^k$) is assumed to be fixed. The equation for determining n_d^k is given in Sec. II D.

The expressions for the charged particle fluxes are[50]

$$\Gamma_e = -D_e \partial_x n_e - n_e \mu_e E, \tag{3}$$

$$\Gamma_i = -D_i \partial_x n_i + n_i \mu_i E, \tag{4}$$

$$\Gamma_- = -D_- \partial_x n_- - n_- \mu_- E, \tag{5}$$

where $D_\alpha = T_\alpha / m_\alpha \nu_{\alpha n}$ and $\mu_\alpha = D_\alpha / T_\alpha$ are the diffusion and mobility coefficients, respectively. Here, E is the ambipolar electric field, and $\nu_{\alpha n}$ are the effective rates of momentum transfer of the species α.

Taking into account plasma quasineutrality (1) and balance of the charged-particle grain currents (2), one can eliminate E and n_- in Eq. (4) to obtain the following expressions for the electrons and positive ions

$$\Gamma_e = -[\mu_i n_i + \mu_-(n_i - n_e + \Sigma_k n_d^k Z_d^k)] D_e \zeta^{-1} \partial_x n_e - \mu_e n_e (D_i \partial_x n_i - \chi D_-) \zeta^{-1}, \tag{6}$$

$$\Gamma_i = -[\mu_e n_e + \mu_-(n_i - n_e + \Sigma_k n_d^k Z_d^k)] D_i \zeta^{-1} \partial_x n_i - \mu_i n_i (D_e \partial_x n_e + \chi D_-) \zeta^{-1}, \tag{7}$$

fluxes, respectively, where $\zeta = (\mu_i + \mu_-) n_i + (\mu_e - \mu_-) n_e + \mu_- \Sigma_k n_d^k Z_d^k$, and $\chi = \partial_x (n_i - n_e + \Sigma_k n_d^k Z_d^k)$.

The conservation equations for the electrons, positive and negative ions are

$$\partial_t n_e + \partial_x \Gamma_e = \nu^i n_e - \nu_{\text{att}} n_e - \Sigma_k \nu_{ed}^k n_d^k, \tag{8}$$

$$\partial_t n_i + \partial_x \Gamma_i = \nu^i n_e - K_{\text{rec}} n_i n_- - \Sigma_k \nu_{id}^k n_d^k, \tag{9}$$

$$\partial_t n_- + \partial_x \Gamma_- = \nu_{\text{att}} n_e - K_{\text{rec}} n_i n_- - \Sigma_k \nu_{-d}^k n_d^k, \tag{10}$$

where ν^i and ν_{att} are ionization and attachment rates, respectively, K_{rec} is positive–negative ion recombination coefficient, and $\nu_{\alpha d}^k$ is the frequency with which a plasma particle of species α attaches to a powder particle of charge Z_d^k. The expression for the frequency is presented in Sec. II D.

Applying Eq. (1), one can eliminate the number density of the negative ions from the positive-ion balance Eq. (9) to obtain

$$\partial_t n_i + \partial_x \Gamma_i = \nu^i n_e - K_{\text{rec}} n_i (n_i - n_e + \Sigma_k n_d^k Z_d^k) - \Sigma_k \nu_{id}^k n_d^k, \tag{11}$$

which will be needed in the numerical analysis.

Power balance in the electronegative plasma is given by[51]

$$\tfrac{3}{2} n_e \partial_t T_e + \partial_x q_e \approx -n_e J_e + S_{\text{ext}}, \tag{12}$$

where $q_e \approx -5 n_e T_e / (2 m_e \nu_{en}) \partial_x T_e$ is the heat flux density, and

$$J_e = \sum_j \nu_j \mathcal{E}_j,$$

is the collision integral of the electrons. Here, ν_j is the rate for collisions of electrons with other particles and $\mathcal{E}_j$ is the energy loss in the collisions. Since the powder density is

TABLE I. Dependencies of the electron(ion)-neutral collision coefficients (in cm^3/s) on electron temperature T_e (in eV) used as input for the fluid model.

Quantity	Functionality
Electron neutral collision coefficient for momentum transfer	$K_{en}=10^{-7}(-0.26+1.67T_e-0.54T_e^2+0.09T_e^3-0.0059T_e^4)$
Ionization coefficient (threshold energy $U^i=11.6$ eV)	$K^i=3.07\times10^{-8}T_e^{0.68}\times\exp(-U^i/T_e)$
Coefficient for vibration excitation with threshold energy $U_{v1}=0.113$ eV	$K_{v1}=10^{-8}(-0.66+4.76T_e-2.09T_e^2+0.38T_e^3-0.026T_e^4)$
Coefficient for vibration excitation with threshold energy $U_{v2}=0.271$ eV	$K_{v2}=10^{-8}(-1.12+6.15T_e-3.48T_e^2+0.97T_e^3-0.15T_e^4+0.012T_e^5-3.82\times10^{-4}T_e^6)$
Coefficient for electronic excitation with threshold energy $U_{exc}=8.0$ eV	$K_{exc}=9.0\times10^{-8}T_e^{0.5}\times\exp(-U_{exc}/T_e)$
Attachment coefficient	$K_{att}=4.1\times10^{-10}T_e^{-0.72}\times\exp(-7.0/T_e)$
Positive–negative ion recombination coefficient[a]	$K_{rec}=2.0\times10^{-7}$
Ion-neutral collision coefficient[b]	$K_{in}=\sigma_{in}[v_i^2+8T_i/\pi m_i]^{1/2}$, where $\sigma_{in}=6.0\times10^{-15}$ cm^{-2}

[a]Reference 26.
[b]Reference 53.

small compared with the neutral particle density, it can be assumed that the energy lost by electron-neutral collisions is dominant.

The plasma electrons are heated by the rf fields, the Joule heating term S_{ext} in Eq. (12) is[51]

$$S_{\text{ext}}\approx n_e\nu_{en}m_e u_{\text{osc}}^2,$$

where u_{osc} is the time-averaged oscillation velocity of the electrons in a rf field.

Quasistationary state of the plasma corresponds to setting $\partial_t=0$ in all the equations. Our approach is valid for fixed rf power absorption P_{in} per unit area, with

$$P_{\text{in}}=\int_{-L/2}^{L/2}S_{\text{ext}}dx,$$

and for determining the electron-neutral collision rates in Eqs. (8)–(10) and (12), the dependence of the rate coefficients on the electron temperature is found using the cross sections for SiH_4 electron-neutral collisions[52] and assuming Maxwellian electron energy distribution. They are presented in Table I.

C. Boundary conditions

The boundary conditions needed for integrating Eqs. (8), (11), (12) are now discussed. Because of the symmetry of the discharge, the gradients of the electron temperature and electron/ion number densities are zero at $x=0$. Since the plasma is ambipolar, at the slab edges ($x=\pm L/2$) the electron and positive-ion fluid velocities are equal to the Bohm speed $v_B=\sqrt{T_e n_i/m_i n_e}$.[50]

The boundary conditions for the electron heat flow are[51]

$$q_e(\pm L/2)=T_e(\pm L/2)(2+\ln\sqrt{m_i/m_e}), \tag{13}$$

$$\times n_e(\pm L/2)\sqrt{T_e(\pm L/2)/m_i}, \tag{14}$$

and since the negative ion temperature is much lower than that of the electrons, the negative ion flux at the negatively charged discharge walls is small compared to that of the electrons and can thus be neglected.

D. Particle charging

It is believed that the nanoparticles are charged mainly by collection of electrons and positive ions. Negative ions can also attach to the nanoparticles, and together with the electrons they bring negative charge onto the grains. However, since $T_i\ll T_e$, the negative ion flux at the grain is much smaller than the electron flux and can thus be neglected.

We recall that in the powder size range considered ($\sim$10 nm) quantum effects in the attachment process are unimportant. The electron and ion fluxes at the grain can be described by the OML probe theory.[37–39] The rates at which a grain with charge $Z_d^k=ke$ collects electrons and ions are then[37–39]

$$\nu_{ed,id}^k=n_{e,i}\pi a_d^2 u_{e,i}\exp(-q_{e,i}Z_d^k/a_d\epsilon_{e,i}), q_{e,i}Z_d^k\geqslant 0$$

$$\nu_{ed,id}^k=n_{e,i}\pi a_d^2 u_{e,i}(1-q_{e,i}Z_d^k/a_d\epsilon_{e,i}),$$

$$q_{e,i}Z_d^k<0 \tag{15}$$

where $u_e=(8T_e/\pi m_e)^{1/2}$, $\epsilon_e=T_e$, a_d is the fine particle radius, $q_{e,i}=\mp e$ is the electron and ion charge, respectively. Taking into account that the drift velocity ($v_i=\Gamma_i/n_i$) of the positive ions can be equal or larger than the ion thermal velocity, we have $u_i=(v_i^2+8T_i/\pi m_i)^{1/2}$ and $\epsilon_i=m_i u_i^2/2$.

The charge distribution of grains of radius a_d is described by the fraction F_k of grains carrying the charge ke. In the steady state the recursive relation for the charge distribution is[37]

$$F_{k+1}=F_k\nu_{id}^k/\nu_{ed}^{k+1}, \tag{16}$$

so that starting with any F_k and taking into account the normalization $\Sigma_k F_k=1$ one can find from Eq. (16) the charge distribution of the powder particles. Thus, at powder density n_d, the concentration n_d^k of powder particles having charge Z_d^k is $F_k n_d$. Photodetachment of electrons from the grains by UV radiation, secondary electron emission due to energetic electrons in the sheaths of rf discharges, and detachment due to quenching of excited atoms at the grain surface can also affect the particle charge and plasma properties.[37] The effect of the UVPD processes on the powder and discharge parameters will be discussed in Sec. III E.

E. Numerical method

The set of equations describing nanoparticle-loaded electronegative plasmas given in Sec. II is highly nonlinear and its solution requires rigorous numerical routines. Our numerical code consists of two major blocks describing a two-step solution process.

The integration begins with a guessed initial plasma state, followed by a two-step calculation cycle. The initial

profiles of $n_{i,e}$, $\Gamma_{i,e}$, T_e, and $\langle Z_d \rangle$ (where $\langle Z_d \rangle \equiv \Sigma_k n_d^k Z_d^k / n_d$) are estimated from earlier rough analytical or computational estimates. From the guessed powder CDF the profiles of the electron/positive ion densities and velocities, as well as the electron temperature, are computed from Eqs. (8), (11), and (12). Then, using the calculated plasma parameters the powder CDF is calculated from Eq. (16). The cycle is repeated until the parameters become constant within a prescribed tolerance.

The governing Eqs. (8), (11), and (12) are solved using a finite difference scheme based on the balanced integrointerpolation method.[54] A detailed description of the numerical method can be found in Ref. 55. The computation is carried out for parameters (pressure range, plasma size, input power, and powder size and density) typical in modern ICP reactors[56,57] and experiments on fine powders in silane-based plasmas.[49]

III. RESULTS

The interdependence of the characteristics of the nanoparticles and the discharge plasma are of particular interest in this section. We vary either the powder parameters (size and density) or the discharge control parameters (input power P_{in} and neutral gas pressure p_0) and monitor the variations of the nanoparticle CDF and the discharge characteristics (electron density and temperature, and positive and negative ion densities). The study is carried out for powders with radii of 5, 7, and 10 nm at densities $n_d = 10^6 - 2.0 \times 10^9$ cm^{-3}. Formation of particles with such sizes and densities is typical for laboratory silane plasmas. For example, in the experiment of Boufendi and Bouchoule[49] the formation of 10 nm powder with $\sim 2 \times 10^9$ cm^{-3} was observed (see Fig. 2 of Ref. 49) about 1 s into the discharge. The powder diameter increases gradually at this stage of the discharge, mainly from coagulation of smaller nanoparticles.[1,37]

A. Effect of powder density

To simulate the formation of powder particles, we varied the fine-particle density in our calculations. The study was carried out for a plasma slab with $L = 3$ cm, gas pressure of 100 mTorr, and grain radius of 10 nm. It is assumed that the overall powder density n_d is uniform for $x \leqslant 1$ cm and linearly decreases to zero at $x = 1.5$ cm, as shown in Fig. 1. Dependence of n_i, n_-, $|n_d \langle Z_d \rangle|$ and n_e at $x = 0$ on total powder density n_d are presented in Fig. 2(a). Positive ion density profiles for different nanoparticle densities are shown in Fig. 2(b). One can see that an increase of the fine particle density is accompanied by a drop of electron density and increase of the ion density. The variations of the charged particle densities can be attributed to the effect of the nanoparticles on the electron temperature and on the diffusion of positive ions. Indeed, the electron temperature is 1.49, 1.62, and 1.72 eV for the fine particle densities 10^8, 5×10^8, and 10^9 cm^{-3}, respectively. The growth of the electron temperature is due to the additional loss of electrons to the powder particles. Since the total surface of the powder particles rises with the powder density, the number of electrons collected by the particles also increases. The electron loss is compensated by enhanced ionization through increase of T_e. Thus, at fixed input power, the growth of the nanoparticles is accompanied by a drop of the electron density. With increase of the total nanoparticle density, the absolute value $|\Sigma_k n_d^k Z_d^k|$ [curve 3 in Fig. 2(a)] of the (negative) powder charge per unit volume appearing in Eq. (1) also increases. The relative increase ($|\Sigma_k n_d^k Z_d^k / n_i|$) with respect to the positive ion density is maximum near $x = 1$ cm. To maintain quasineutrality of the plasma, the positive ion density also increases in this region, as shown in Fig. 2(b). This increase is accompanied by a decrease of the positive ion density gradient at the central part ($x \leqslant 1$ cm) of the discharge and decrease of positive ion drift velocity [see Fig. 2(c)]. The change in the drift velocity affects the diffusion loss of the positive ions, thus also the absolute value of the positive ion density, which increases weakly with the powder density [see Figs. 2(a) and 2(b)].

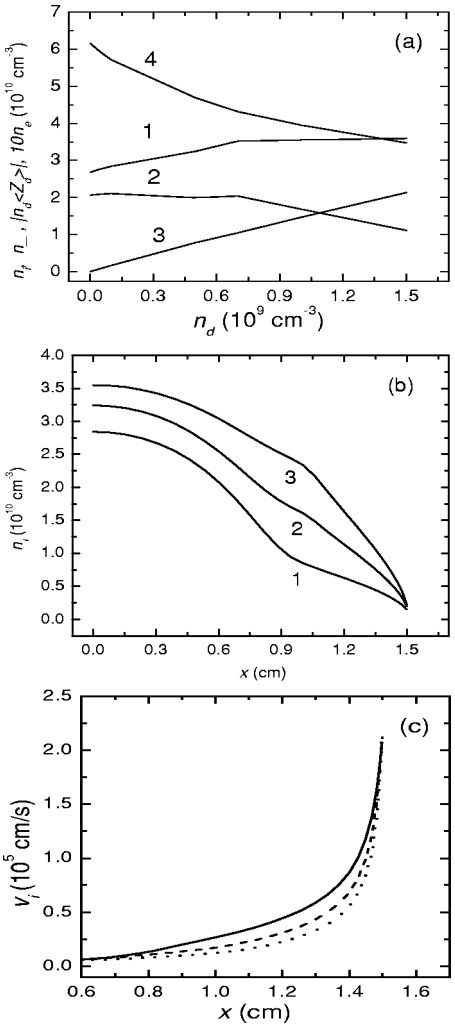

FIG. 2. Positive (1) and negative (2) ion densities, $|n_d \langle Z_d \rangle|$ (3) and $10 \times n_e$ (4) at $x = 0$ in a 100 mTorr discharge sustained plasma slab 3 cm in thickness at a nanoparticle radius $a_d = 10$ nm and an input power $P_{\text{in}} = 0.12$ W/cm^2 in dependence of powder density (a). Profiles of positive ion density (b) and positive ion velocity (c) at the same conditions as in Fig. 2(a). The curves 1, 2, and 3 for n_i in (b), and solid, dashed, and dotted lines in (c) for v_i correspond to $n_d = 10^8$ cm^{-3}, 5×10^8 cm^{-3}, and 10^9 cm^{-3}, respectively.

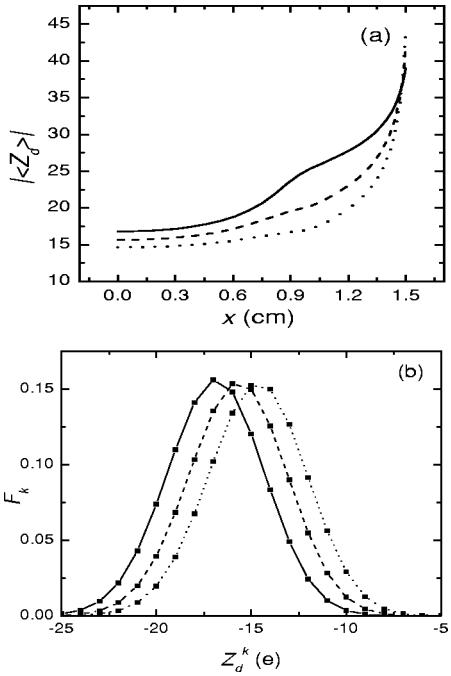

FIG. 3. Profile of $|\langle Z_d\rangle|$ (a) and powder charge distribution function F_k at $x=0.16$ cm for different powder densities. The solid, dashed, and dotted lines correspond to $n_d=10^8$ cm^{-3}, 5×10^8 cm^{-3}, and 10^9 cm^{-3}, respectively. Other conditions are the same as in Fig. 2.

Figure 2(a) shows that the negative ion density is practically constant at low ($n_d \leqslant 7\times10^8$ cm^{-3}) powder densities, and it drops when n_d becomes higher. This nonlinear behavior of n_- may be explained as follows: at low powder densities the effect of the nanoparticle on the negative ions is small, and n_- depends mainly on electron attachment. The latter is enhanced by increase of the electron temperature, and weakened by decrease of the electron density. Since with increase of the powder density, T_e grows and n_e drops, the negative ion density is practically constant at low nanoparticle densities, as can be seen in Fig. 2(a), but with the increase of n_d, the nanoparticles can strongly affect the negative ion density. Because the positive ion density changes only slightly with powder density, and the discharge is quasineutral [Eq. (1)], the growth in n_d is accompanied by decrease of n_- for $n_d>7\times10^8$ cm^{-3} [see Fig. 2(a)].

As expected, the decrease of electron density with increase of the powder density is accompanied by a decrease of the average negative charge on the fine grains, as shown in Fig. 3(a). Therefore, the powder CDF shifts in the direction of lower negative charge as the powder density increases, as can be seen in Fig. 3(b). The maximum of the CDF as well as its FWHM are practically independent of the powder density.

B. Effect of powder size

In this section, we study the effect of the powder size variation on the plasma and other powder parameters. This roughly models the size growth of the nanoparticles. In Figs. 4(a)–4(c) the density profiles of the plasma species are shown for the powder radii 5, 7, and 10 nm.

Figures 4(a) and 4(b) show that the electron density decreases as the powder size increases, while the positive ion density increases slightly and its profile becomes flatter in central region of the plasma. This behavior can be attributed to the variation of the electron temperature and powder charge with the powder diameter: T_e is 1.53, 1.64, and 1.83 eV for powder radii of 5, 7, and 10 nm, respectively. Physically, this is because a larger powder surface area supports higher loss of the plasma electrons that have to be reinstated by higher rate ionization at increased electron temperature. An increase of the electron temperature also leads to increase of the collision integral J_e in Eq. (12), and for constant $P_{\rm in}$ it has to be accompanied by a decrease of the electron density.

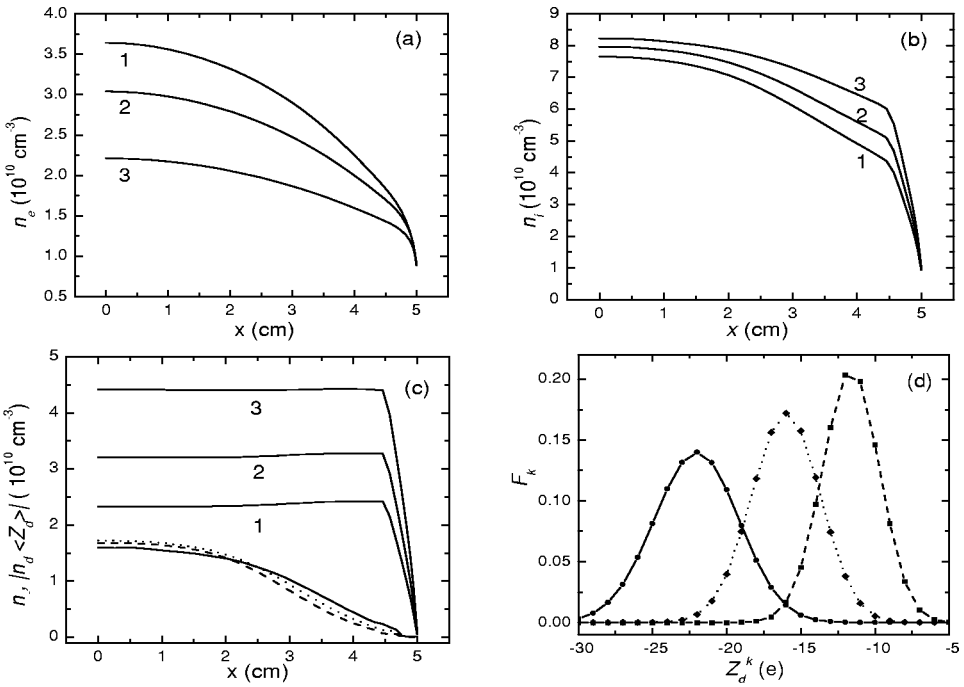

FIG. 4. Profiles of n_e (a), n_i (b), and $|n_d\langle Z_d\rangle|$ (c) in a 10 cm wide plasma slab at $P_{\rm in}=1.2$ W/cm^2, $p_0=50$ mTorr, $n_d=2\times10^9$ cm^{-3} for the nanoparticle radii: (1) 5 nm, (2) 7 nm, and (3) 10 nm. The dashed, dotted, and solid lines in (c) for n_-, as well as in (d) for F_k (at $x=0.52$ cm) correspond to $a_d=5$, 7, and 10 nm, respectively.

As the grain surface area grows, the average powder charge increases [Fig. 4(d)]. Therefore, the charge per unit volume $|\Sigma_k n_d^k Z_d^k|$ also increases. This then leads to the increase of n_i and the shoulders in its profile. The reasons for the increase are the same as that occurring when the powder density is increased (see Sec. III A).

For the plasma parameters considered here, the negative ion density is practically independent of the powder size [Fig. 4(c)]. This may be attributed to the fact that the creation of negative ions in the discharge is by attachment of electrons to neutral atoms [see Eq. (10)], and is thus dependent only on the electron density and temperature. Lowering the electron density leads to lowering of the negative ion density, and vice versa. Raising T_e will increase the production of powder. As the powder size increases, the electron density will be lowered and the electron temperature increased, thus leaving n_- practically independent of a_d. We note that with the decrease of the powder radius, the powder CDF becomes sharper and shifts towards smaller negative charge [see Fig. 4(d)].

C. Effect of input power

Here we consider the possibility of management of powder and discharge properties through input power P_{in} control. We vary P_{in} and observe the behavior of the nanoparticles and the discharge properties. The dependencies of n_e, n_i, n_-, and $|\langle n_d Z_d \rangle|$ at $x=0$ on P_{in} are depicted in Fig. 5(a). One can see that an increase of the power is accompanied by a rise of the positive and negative ion densities, and an even stronger rise in the electron density. When P_{in} increases from 0.3 to 4.8 W/cm^2, n_e, n_i, n_- increases from 2.6, 36.1, and 8.49×10^9 cm^{-3} to 7.3, 15.2, and 3.1×10^{10} cm^{-3}, respectively. One can see from Fig. 5(a) that n_i and n_- increase with the input power faster at low powers. This is because the positive ion density is higher than that in the powder-free discharge under the same conditions, and it increases with the powder density. Another process that affects the positive ion density is positive–negative ion recombination. Since the latter increases with the input power, the growth of n_i will be somewhat weaker at higher powers. This behavior occurs only in plasmas with negative ions and charged grains.

For the parameters of Fig. 5, the electron temperature at the discharge midplane $x=0$ is 1.83, 1.63, and 1.6 eV for $P_{\text{in}}=0.3$, 2.4, and 4.8 W/cm^2, respectively. Enhancement of the electron temperature with power drop is in our opinion due to additional electron loss to the nanoparticles. If powder density is kept constant, the relative fine particle density with respect to n_e increases at lower input powers. Therefore, with power decrease the proportion of the plasma electrons collected by the powder particles increases with respect to that absorbed by the discharge walls. The complex plasma then self-organizes to compensate for the additional electron loss by increasing ionization and the electron temperature.

The positive-ion density profiles n_i for different power absorbed per unit area are shown in Fig. 5(b). Similar to the case of powder-size increase discussed in Sec. III B, the n_i profile becomes significantly flatter when the power decreases (nanoparticle effect increases). Since the density of the electrons taking part in the electron-neutral attachment process grows with power input, the negative-ion density also rises [curve 3 in Fig. 5(a)]. The averaged powder charge increases with the power input [Figs. 5(a) and 5(c)]. This may be attributed to a rise of the electron and ion fluxes at the nanoparticles at higher powers. However, the maximum of the powder CDF decreases slightly with power input.

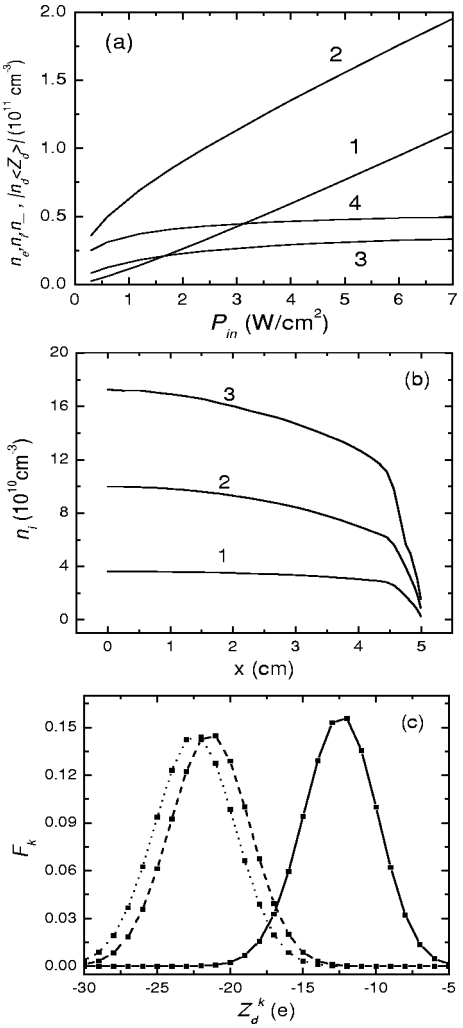

FIG. 5. Electron (1), positive (2), and negative (3) ion densities, and $|n_d\langle Z_d\rangle|$ (4) at $x=0$ for $p_0=100$ mTorr, $n_d=2\times10^9$ cm^{-3}, and $a_d=10$ nm in dependence on input power P_{in}. Positive ion density profile (b) and F_k (c) at $x=0.52$ cm for the same conditions as in (a). The curves 1–3 for n_i in (b), and solid, dashed, and dotted lines in (c) for F_k correspond to $P_{\text{in}}=0.3$, 2.4, and 4.8 W/cm^2, respectively.

D. Effect of neutral gas pressure

The effect of the neutral gas pressure on the electrons and ions, as well as the powder CDF, are also investigated. The profiles of the charged particle densities are shown in Figs. 6(a)–6(c) for different neutral gas pressures in the range from 50 to 200 mTorr. One can see in Figs. 6(a) and 6(b) that an increase of the pressure is accompanied by decreases in the electron and positive-ion densities. The electron temperature also decreases with the pressure (e.g., T_e at $x=0$ is 1.57, 1.69, and 1.83 eV for pressures of 200, 100, and 50 mTorr, respectively). We recall that in electropositive

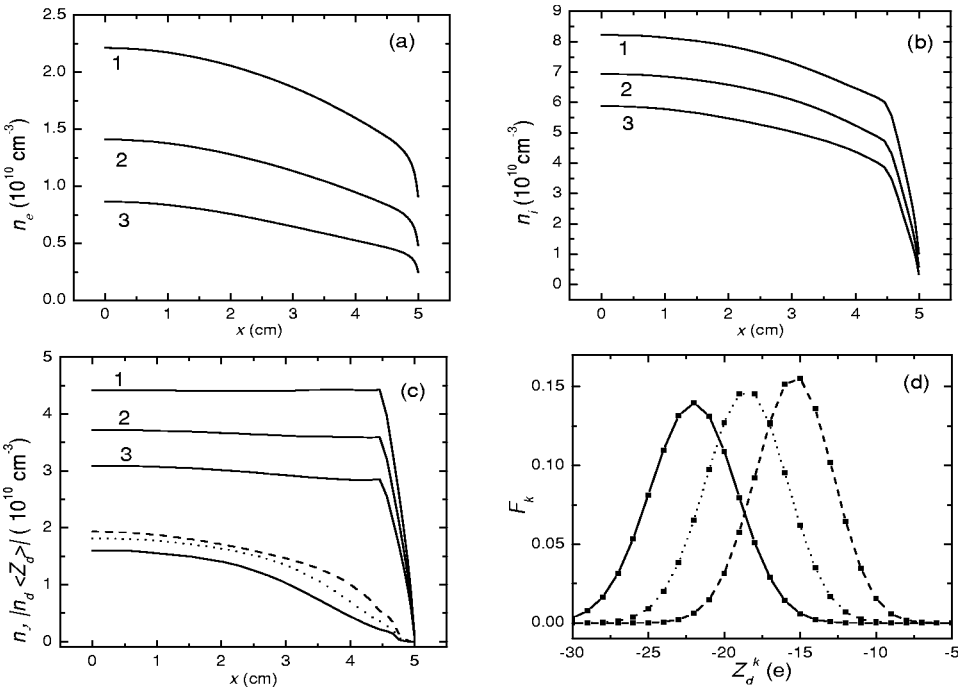

FIG. 6. Profiles of n_e (a), n_i (b), and $|n_d\langle Z_d\rangle|$ (c) for $P_{\text{in}}=1.2$ W/cm^2 and neutral gas pressures 50 mTorr (curve 1), 100 mTorr (curve 2), and 200 mTorr (curve 3). The solid, dotted, and dashed lines in (c) for n_-, and in (d) for F_k (at $x=0.52$ cm) correspond to $p_0=50$, 100, and 200 mTorr, respectively. The other conditions are the same as in Fig. 5.

argon plasmas, pressure increase is usually accompanied by an increase of the electron density and decrease of the electron temperature (see, e.g., Fig. 6 of Ref. 55). We believe that the reason for the decrease of the electron density (silane plasma) is that here the electron collision integral J_e in Eq. (12) increases with pressure. One can show that in the parameter range of interest the main power loss is from vibrational excitation of the silane molecules. Owing to the rather low energy threshold (0.1–0.3 eV) for the process, the major collision rates are somewhat less sensitive to the electron temperature dependence on p_0 than to the change in the density of the neutrals.

Contrary to the electron and positive ion densities, the negative ion density increases slightly with pressure. The growth of n_- may be attributed to the decrease in positive–negative ion recombination as described by the term $n_i n_- K_{\text{rec}}$ in Eq. (10) since n_i decreases with the pressure. Figure 6(d) shows that because of electron density and temperature decrease, the average powder charge also decreases with the pressure. However, the maximum of the powder CDF increases slightly.

E. Effect of photodetachment of electrons

The nanopowder charging process can also be affected by photodetachment of electrons due to UV photons, secondary electron emission due to energetic electrons in the sheaths, and electron detachment due to quenching of excited atoms at the powder surface. Taking into account these processes, one can rewrite the recursive relation for the nanoparticle CDF in Eq. (16) as[37]

$$F_{k+1}=F_k(\nu_{id}^k+\nu_\gamma+\nu_{qu}+\nu_{se})/\nu_{ed}^{k+1}, \tag{17}$$

where ν_γ, ν_{qu}, and ν_{se} are the charging rates due to resonant UVPD of electrons, quenching of excited atoms, and secondary electron emission, respectively. In typical laboratory electronegative plasmas with nanoparticles,[49] we have $\nu_\gamma \gg \nu_{qu}, \nu_{se}$, as shown in Fig. 8 of Ref. 37. Therefore, we will consider only the effect of UV photodetachment on the charge of the nanoparticles and the plasma properties. We vary the charging frequency ν_γ and follow the electron temperature, electron/ion densities, and powder CDF. Determination of the frequency ν_γ is rather complicated,[37] and because of a lack of information on the Si:H particles, ν_γ is usually estimated only qualitatively. Photodetachment of electrons from the nanoparticles can also affect electron balance in the discharge. To take into account the effect, the term $\nu_\gamma n_d$ was added to the right-hand side of the electron balance Eq. (8).

In the numerical evaluation, the charging rates $\nu_\gamma = 10^3, 10^5, 10^6 \times n_e/n_e(0)\,\text{s}^{-1}$, were considered, where $n_e(0)$ is the electron density at $x=0$. The term $n_e/n_e(0)$ in the expression for ν_γ is to account for the spatial nonuniformity of the excited atoms [see Eqs. (4) and (19) of Ref. 37] and thus the nonuniformity of ν_γ. The rates used here are consistent with the range (10^3–10^6 s^{-1}) obtained in Ref. 37 for the experimental conditions of Ref. 49.

The equilibrium spatial profiles of the plasma particle densities at different photodetachment frequencies are shown in Figs. 7(a)–7(c). For the parameters of Fig. 7, the electron temperature at the discharge midplane $x=0$ is 1.83, 1.82, and 1.72 eV for $\nu_\gamma = 10^3, 10^5$, and $10^6 \times n_e/n_e(0)$ s^{-1}, respectively. One can see that increase of photodetachment is accompanied by decrease of the electron temperature and average powder charge [Fig. 7(c)]. This behavior can be interpreted as follows: if UVPD is increased at constant power input P_{in}, electrons are removed from the nanoparticles, so that the free electron density in the discharge increases, as can be seen in Fig. 7(a). Thus, the number of electrons taking part in the ionization of the neutrals increases with UVPD, so

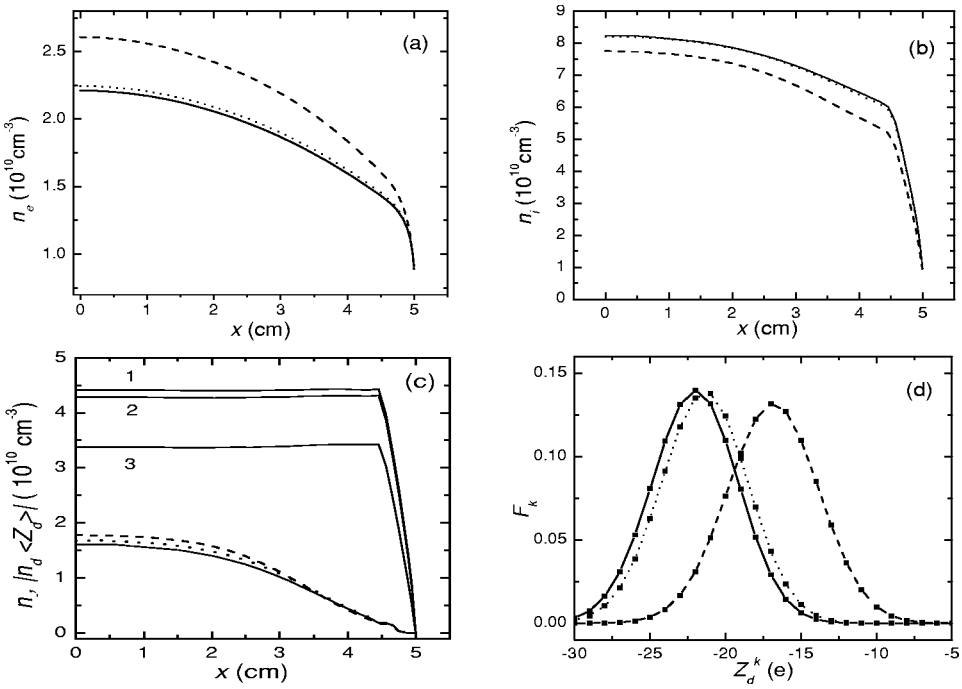

FIG. 7. Same as in Fig. 6, but for $p_0 = 50$ mTorr and UV photodetachment rates $\nu_\gamma = 10^3 n_e/n_e(0)$ s^{-1} (solid line), $10^5 n_e/n_e(0)$ s^{-1} (dotted line), and $10^6 n_e/n_e(0)$ s^{-1} (dashed line). The curves 1–3 in (c) for $|n_d\langle Z_d\rangle|$ correspond to $\nu_\gamma = 10^3 n_e/n_e(0)$ s^{-1}, $10^5 n_e/n_e(0)$ s^{-1}, and $10^6 n_e/n_e(0)$ s^{-1}, respectively. The other parameters are the same as in Fig. 6.

that a lower electron temperature is needed to maintain the diffusion equilibrium in the plasma.

Since with the increase of UVPD of electrons from the nanoparticles, the growth of ν_γ is accompanied by diminishing of the averaged negative charge accumulated on the particles, as can be seen in Fig. 7(d). Because of the charge drop the effect of the powder particle on the positive ion profile weakens as UVPD of electrons increases, and the positive ion density becomes lower, especially near $x = 4.5$, where the effect of the nanoparticles is more essential. The density of the negative ions remains practically independent of ν_γ in the parameter range of interest. Figure 7(d) also shows that the maximum of the grain CDF decreases slightly with increase of UVPD. This agrees with results reported by Kortshagen *et al.*[37]

IV. DISCUSSION AND CONCLUSION

In this section we will summarize our main results and comment on their significance and possible applications. From the results of Sec. III one can conclude that the plasma parameters such as the electron temperature and the electron/ion densities, can be managed by controlling the external parameters such as the input power and neutral gas pressure. Furthermore, the discharge properties depend strongly on the size of the powder particles and their concentration. In particular, the electron temperature in a SiH_4 discharge can be lowered by elevating the neutral gas pressure or decreasing the powder size or its density. In contrast to a powder-free plasma, the electron temperature in the electronegative discharge containing nanosize particles of fixed density and size will increase when the input power decreases. This is attributed to an increase in the relative number of electrons collected by powder grains compared to that deposited on the chamber walls.

Electron temperature control is important in many processing plasmas. In fact, the quality of PECVD-fabricated silicon films depend strongly on T_e. To obtain a high quality film one has to keep T_e low.[25] Increase of the deposition rate in PECVD is possible by raising T_e in the plasma reactor.[8] To manage powder growth one also has to control the T_e, by speeding up or slowing down the growth process through increasing or decreasing T_e, respectively.

The computations also show that the SiH_3^- anion (here assumed to be the powder precursor) number density can be efficiently managed. In particular, the anion density may be increased by raising the input power [Fig. 5(a)] or the neutral gas pressure [Fig. 6(c)]. With increase of the powder concentration the density of the ions decreases [Fig. 2(a)]. For the parameter regime of interest the nanoparticle size practically does not affect the density of the powder precursor [Fig. 4(c)]. Control of the number density and reactivity of the SiH_3^- powder precursors in silane plasmas[1,26] should be useful for reducing dust contamination in the manufacturing of integrated circuits. By decreasing the density of the SiH_3^- anions, one can suppress the initial protoparticle nucleation process leading to powder growth.

From the results of our study it follows that the uniformity of positive ion density may also be controlled by changing the external parameters as well as the powder properties. An increase of relative negative powder charge per unit volume with respect to positive ion density ($|\Sigma_k n_d^k Z_d^k/n_i|$) is accompanied by a flattening of the n_i profile in the central part of the discharge. The ratio ($|\Sigma_k n_d^k Z_d^k/n_i|$) maximizes near the discharge boundary, where the ion density drops due to ion diffusion to plasma walls. To maintain quasineutrality of the plasma the positive ion density increases, which is however accompanied by a decrease of the gradient of n_i in the central part of the discharge. Thus, the positive ion density profile becomes flatter at higher powder densities, as

shown in Fig. 2(b). The uniformity of n_i improves with an increase of the powder size [Fig. 4(b)] and a decrease of the input power [Fig. 5(b)]. We emphasize that the uniformity of the ion density is important for many plasma assisted etching and deposition applications.[50]

Furthermore, one can also manage the powder CDF by controlling the external parameters. Indeed, the magnitude of the average powder charge can be enhanced by increasing the input power and lowering the neutral gas pressure [Figs. 5(c) and 6(d)]. With growth of $|\langle Z_d \rangle|$, the FWHM of the powder CDF increases. This agrees with observations (see Ref. 40 and the references therein), where it was found that the averaged particle charge and its fluctuation increase together. The magnitude of the charge increases as the powder surface area increases [Fig. 4(d)], but it decreases with the powder density [Fig. 3(a)]. Detailed knowledge of the powder charge is important in integrated circuit manufacturing. Raising the powder charge one can manage conditions for levitation of the particles to prevent their harmful drop onto the wafer.

UVPD of electrons from the nanoparticles can strongly affect the average powder charge and the plasma properties. Intensifying UVPD reduces the number of electrons on the nanoparticles, and thus increases [Fig. 7(a)] n_e, and decreases T_e and the powder charge. Because of a lack of information on the Si:H nanoparticles, the effect of UVPD has been studied only qualitatively here. However, this process is clearly important for accurate modeling of an electronegative plasma with nanoparticles. Further experimental and theoretical investigations of the particle properties, especially the charging of the nano- and subnano-particles are clearly warranted.

We now discuss the validity of the main assumptions used in this study. First, the powder size and density are external parameters (although based on experimental values) in our discharge model. To predict their dependence on the neutral gas pressure and temperature, and plasma volume, a detailed study of the powder growth process[29,37] is required. For simplicity, processes in the plasma sheaths as well as the powder dynamics have not been considered. Accounting for these complex processes could somewhat improve our model of the electronegative discharge.

In this study, the charged nanoparticles were treated as immobile point masses with the invariable number density. We have also assumed that the discharge is steady and that the powder size is fixed, which is often not the case in real chemically active plasmas.[1] In reality, the variously charged dusts are generated in silane discharges as a result of complex chemical reactions of anions or radicals with SiH_4 molecules and lost to the pumping and diffusion processes. In most powder-generating discharges the nanoparticle loss process is somewhat slower than the generation one and the dust size and number density increase in time.[49,58] In this sense the dust-contaminated discharges are nonstationary and the growing dusts dynamically affect the number densities of the plasma electrons and ions. However, the characteristic time scales for the nanoparticle size and density variations τ_{NP} are much longer than those for the electron/ion losses due to the recombination and diffusion. For example, only a minor ($\sim 1\%$) variation of the fine particle density over the time scales $\tau_{NP} \sim 10$ ms was reported for typical silane discharges.[49] Therefore, the process of powder growth in the silane plasma may be treated as quasistationary in the model.

The characteristic time of the powder diffusion in a parallel plate discharge geometry can be estimated[59] by $\tau_D = L^2/D_d\pi^2$, where $D_d \approx 14\, a_d^{-2} p_0^{-1}$ cm^2 s^{-1} is the nanoparticle diffusion coefficient, a_d is in nm, and p_0 in Torr. Apparently, τ_D greatly exceeds the ion diffusion time in the electronegative plasmas[50] $\tau_i = L^2/D_i\pi^2$, where $D_i = 2T_i/m_i\nu_{in}$. For the typical conditions of our simulations $\tau_i \approx 5\times 10^{-4}$ s. Therefore, the time scales for the dust size variation and motion/diffusion are much longer as compared with the corresponding time scales of the establishment of the discharge equilibrium state controlled by much faster electron/ion creation and loss processes. Hence, the electrons and ions dynamically reach the equilibrium at any slowly variable powder size and density, which justifies the assumption of the overall charge neutrality in Eq. (1).

It is also notable that the focus of this article is on the various processes in the ionized gas phase involving nanosized particles. The balance/conversion of the neutral species was not included in the model and SiH_4 was assumed a sole neutral species in the discharge. Despite the abundance of various neutral radicals in real silane-based discharges, our model remains accurate when the silane gas conversion into radical and ionic products is inefficient. This situation is quite typical for many thin film deposition processes in undiluted silane disharges.[7] The specifics of the neutral species can nevertheless affect the collision and creation/sink rates of the plasma species. However, inclusion of monomer radicals (e.g., SiH, SiH_2, and SiH_3) would only marginally affect the results of our computations due to low number densities of the radicals and small mass and cross-section difference with the SiH_4 molecules. Furthermore, the positive SiH_3^+ and negative SiH_3^- ions of our model are predominantly generated as a result of the electron impact processes involving SiH_4.

We now discuss the situations when incorporation of the neutral radicals in the model is crucial. For example, neutral radicals, such as SiH_3, are the key species in the deposition of *a*-Si, hydrogenated silica and other silicon-based fims in low-pressure discharges in pure SiH_4.[60–62] Besides, highly reactive neutral radicals such as SiH_2, can efficiently support the gas-phase nanopowder nucleation and growth processes in dense argon-diluted silane plasmas.[29] However, the detail modeling of these processes is outside the scope of this article.

Here, we have used the OML model for the charging of relatively large (~ 10 nm) nanoparticles. We note, however, that the OML theory is not applicable for particles a few nanometers in size.[1,29] In this range the electron collection rate depends not only on the size, but also on the electronic surface structure of the nanograin. For example, Fridman *et al.*[26] found that vibrational excitation can play an important role in the electron-powder attachment process. In such cases, a quantum treatment is required.[1]

On the other hand, our model of the complex electronegative SiH_4 discharge plasma containing nanopowder ac-

counts for the major physical effects such as plasma particle sources and sinks in the system. We note that existing models[26,37] considered averaged plasma parameters, and we investigated self-consistently the cross-sectional profiles of the governing quantities. The model can be straightforwardly extended to other reactive plasmas containing charged powder, such as the hydrocarbon-[3] and fluorocarbon-based[63] powder generating systems.

In summary, we have studied the role of the plasma parameters in the management of nanosize powder particles in a low-pressure parallel-plate silane discharge. The spatial profiles of the electron and positive/negative ion densities, electron temperature, and powder CDFs have been computed for various external and plasma parameters using a self-consistent fluid model. It is shown that the input power, working gas pressure, powder size, and density strongly affect the electron temperature, electron/ion density, and spatial uniformity of the positive ion density. We have shown that one can optimize the parameters to minimize the generation of the negative ion precursors of the fine powder and the required electron temperature. It is also demonstrated that in the presence of the nanoparticles positive ion density profiles with high uniformity can be obtained by controlling the neutral gas pressure, input power, powder size, and its density. Furthermore, powder CDFs can also be managed through control of the external discharge parameters.

ACKNOWLEDGMENTS

This work was supported by the ASTAR (Project No. 012 101 00247), and the Flinders Institute for Research in Science and Technology.

[1] *Dusty Plasmas: Physics, Chemistry, and Technological Impacts in Plasma Processing*, edited by A. Bouchoule (Wiley, New York, 1999).
[2] A. Garscadden, B. N. Ganguly, P. D. Haaland, and J. Williams, Plasma Sources Sci. Technol. **3**, 239 (1994).
[3] S. Stoykov, C. Eggs, and U. Kortshagen, J. Phys. D **34**, 2160 (2001).
[4] E. Stoffels, W. W. Stoffels, H. Kersten, G. H. P. M. Swinkels, and G. M. W. Kroesen, Phys. Scr., T **89**, 168 (2001).
[5] K. N. Tu, J. W. Mayer, and L. C. Feldman, *Electronic Thin Film Science for Electrical Engineers and Materials Scientists* (Macmillan, New York, 1992).
[6] H. Kersten, H. Deutsch, E. Stoffels, W. W. Stoffels, G. M. W. Kroesen, and R. Hippler, Contrib. Plasma Phys. **41**, 598 (2001).
[7] J. Perrin, J. Schmitt, C. Hollenstein, A. Howling, and L. Sansonnens, Plasma Phys. Controlled Fusion **42**, B353 (2000).
[8] L. Boufendi and A. Bouchoule, Plasma Sources Sci. Technol. **11**, A211 (2002).
[9] H. Kersten, P. Schmetz, and G. M. W. Kroesen, Surf. Coat. Technol. **108–109**, 507 (1998).
[10] P. Roca i Cabarrocas, J. Non-Cryst. Solids **266**, 31 (2000).
[11] A. Hadjadj, L. Boufendi, S. Huet, S. Schelz, P. Roca i Cabarrocas, H. Estrade-Szwarckopf, and B. Rousseau, J. Vac. Sci. Technol. A **18**, 529 (2000).
[12] R. Martins, H. Aguas, I. Ferreira, V. Silva, A. Cabrita, and E. Fortunato, Thin Solid Films **383**, 165 (2001).
[13] D. G. Schlom, J. H. Haeni, J. Lettieri, C. D. Theis, W. Tian, J. C. Jiang, and X. Q. Pan, Mater. Sci. Eng., B **87**, 282 (2001).
[14] *Structure-Property Relationships of Oxide Surfaces and Interfaces*, edited by C. B. Carter, X. Q. Pan, K. Sickafus, H. L. Tuller, and T. Wood (Materials Research Society, Warrendale, PA, 2001), Vol. 654.
[15] B. T. Liu, K. Maki, Y. So, V. Nagarajan, R. Ramesh, J. Lettieri, J. H. Haeni, D. G. Schlom, W. Tian, X. Q. Pan, F. J. Walker, and R. A. McKee, Appl. Phys. Lett. **80**, 4801 (2002).
[16] F. G. Si and K. N. Tu, Phys. Rev. Lett. **74**, 4476 (1995).
[17] C. N. Liao, C. Chen, and K. N. Tu, J. Appl. Phys. **86**, 3204 (1999).
[18] M. Goto, H. Toyoda, M. Kitagawa, T. Hirao, and H. Sugai, Jpn. J. Appl. Phys., Part 1 **36**, 3714 (1997).
[19] K. Goshima, H. Toyoda, T. Kojima, M. Nishitani, M. Kitagawa, H. Yamazoe, and H. Sugai, Jpn. J. Appl. Phys., Part 1 **38**, 3655 (1999).
[20] T. Kojima, A. Ohishi, H. Toyoda, M. Goto, M. Nishitani, and H. Sugai, Jpn. J. Appl. Phys., Part 1 **40**, 322 (2001).
[21] Y. Watanabe, M. Shiratani, T. Fukuzawa, H. Kawasaki, Y. Ueda, S. Singh, and H. Ohkura, J. Vac. Sci. Technol. A **14**, 995 (1996).
[22] I. I. Beilis, M. Keidar, R. L. Boxman, and S. Goldsmith, J. Appl. Phys. **85**, 1358 (1999).
[23] M. Keidar and I. I. Beilis, IEEE Trans. Plasma Sci. **27**, 810 (1999).
[24] M. Keidar, R. Aharonov, and I. I. Beilis, J. Vac. Sci. Technol. A **17**, 3067 (1999).
[25] M. Takai, T. Nishimoto, M. Kondo, and A. Matsuda, Appl. Phys. Lett. **77**, 2828 (2000).
[26] A. A. Fridman, L. Boufendi, T. Hbid, B. V. Potapkin, and A. Bouchoule, J. Appl. Phys. **79**, 1303 (1996).
[27] E. Furkal, A. Smolyakov, and A. Hirose, Phys. Rev. E **58**, 965 (1998).
[28] A. Smolyakov, V. Godyak, and A. Duffy, Phys. Plasmas **7**, 4755 (2000).
[29] Ch. Hollenstein, Plasma Phys. Controlled Fusion **42**, R93 (2000).
[30] T. Fukuzawa, S. Kushima, Y. Matsuoka, M. Shiratani, and Y. Watanabe, J. Appl. Phys. **86**, 3543 (1999).
[31] V. N. Tsytovich, G. E. Morfill, and H. Thomas, Plasma Phys. Rep. **28**, 623 (2002).
[32] S. V. Vladimirov and V. N. Tsytovich, Phys. Rev. E **58**, 2415 (1998).
[33] K. N. Ostrikov, S. Kumar, and H. Sugai, Phys. Plasmas **8**, 3490 (2001).
[34] K. N. Ostrikov, M. Y. Yu, and H. Sugai, J. Appl. Phys. **86**, 2425 (1999).
[35] S. V. Vladimirov and N. F. Cramer, Phys. Rev. E **62**, 2754 (2000).
[36] A. Gallagher, Phys. Rev. E **62**, 2690 (2000).
[37] U. Kortshagen and U. Bhandarkar, Phys. Rev. E **60**, 887 (1999).
[38] T. Matsoukas, M. Russel, and M. Smith, J. Vac. Sci. Technol. A **14**, 624 (1996).
[39] V. A. Schweigert and I. V. Schweigert, J. Phys. D **29**, 655 (1996).
[40] A. Piel and A. Melzer, Plasma Phys. Controlled Fusion **44**, R1 (2002).
[41] C. Cui and J. Goree, IEEE Trans. Plasma Sci. **22**, 151 (1994).
[42] V. W. Chow, D. A. Mendis, and M. Rosenberg, IEEE Trans. Plasma Sci. **22**, 179 (1994).
[43] M. Rosenberg and D. A. Mendis, IEEE Trans. Plasma Sci. **23**, 177 (1995).
[44] M. Rosenberg, D. A. Mendis, and D. P. Sheehan, IEEE Trans. Plasma Sci. **27**, 239 (1999).
[45] K. N. Ostrikov, M. Y. Yu, and L. Stenflo, Phys. Rev. E **61**, 782 (2000).
[46] M. Yan and W. J. Goedheer, Plasma Sources Sci. Technol. **8**, 349 (1999).
[47] M. J. Kushner, J. Appl. Phys. **63**, 2532 (1988).
[48] U. V. Bhandarkar, M. T. Swihart, S. L. Girshick, and U. R. Kortshagen, J. Phys. D **33**, 2731 (2000).
[49] A. Bouchoule and L. Boufendi, Plasma Sources Sci. Technol. **2**, 204 (1993).
[50] M. A. Lieberman and A. J. Lichtenberg, *Principles of Plasma Discharges and Materials Processing* (Wiley, New York, 1994).
[51] V. E. Golant, A. P. Zhilinskii, and I. E. Sakharov, *Fundamentals of Plasma Physics* (Wiley, New York, 1980).
[52] Kinema Research and Software, http://www.kinema.com/sigmalib.dat
[53] J. P. Boeuf and Ph. Belenguer, J. Appl. Phys. **71**, 4751 (1992).
[54] A. N. Tichonov and A. A. Samarskii, *Partial Differential Equations of Mathematical Physics* (North-Holland, Amsterdam, 1987).
[55] N. A. Azarenkov, I. B. Denysenko, A. V. Gapon, and T. W. Johnston, Phys. Plasmas **8**, 1467 (2001).
[56] K. N. Ostrikov, I. B. Denysenko, E. L. Tsakadze, S. Xu, and R. G. Storer, J. Appl. Phys. **92**, 4935 (2002).
[57] A. B. M. Shafiul Azam, K. N. Ostrikov, S. Xu, Y. Li, and S. Lee, Sing. J. Phys. **16**, 56 (2000).
[58] S. V. Vladimirov and K. Ostrikov, Plasmas Polymers **8**, 135 (2003).
[59] M. A. Childs and A. Gallagher, J. Appl. Phys. **87**, 1076 (2000).
[60] C. C. Tsai, J. C. Knights, G. Chang, and B. Wacker, J. Appl. Phys. **59**, 2998 (1986).
[61] N. Itabashi, N. Nishiwaki, M. Magane, S. Naito, T. Goto, A. Matsuda, C. Yamada, and E. Hirota, Jpn. J. Appl. Phys., Part 2 **29**, L505 (1990).
[62] M. J. McCaughey and M. J. Kushner, J. Appl. Phys. **65**, 186 (1989).
[63] K. Takahashi and K. Tachibana, J. Appl. Phys. **89**, 893 (2001); J. Vac. Sci. Technol. A **19**, 2055 (2001).